

Astrophysical Effects of Scalar Dark Matter Miniclusters

Kathryn M. Zurek, Craig J. Hogan, Thomas R. Quinn

Physics and Astronomy Departments, University of Washington, Seattle, WA 98195

We model the formation, evolution and astrophysical effects of dark compact Scalar Miniclusters (“ScaMs”). These objects arise when a scalar field, with an axion-like or Higgs-like potential, undergoes a second order phase transition below the QCD scale. Such a scalar field may couple too weakly to the standard model to be detectable directly through particle interactions, but may still be detectable by gravitational effects, such as lensing and baryon accretion by large, gravitationally bound miniclusters. The masses of these objects are shown to be constrained by the Ly α power spectrum to be less than $\sim 10^4 M_\odot$, but they may be as light as classical axion miniclusters, of the order of $10^{-12} M_\odot$. We simulate the formation and nonlinear gravitational collapse of these objects around matter-radiation equality using an N-body code, estimate their gravitational lensing properties, and assess the feasibility of studying them using current and future lensing experiments. Future MACHO-type variability surveys of many background sources can reveal either high-amplification, strong lensing events, or measure density profiles directly via weak-lensing variability, depending on ScaM parameters and survey depth. However, ScaMs, due to their low internal densities, are unlikely to be responsible for apparent MACHO events already detected in the Galactic halo. As a result, in the entire window between $10^{-7} M_\odot$ and $10^2 M_\odot$ covered by the galactic scale lensing experiments, ScaMs may in fact compose all the dark matter. A simple estimate is made of parameters that would give rise to early structure formation; in principle, early stellar collapse could be triggered by ScaMs as early as recombination, and significantly affect cosmic reionization.

I. INTRODUCTION

Despite experimental efforts to ascertain the nature of dark matter, its fundamental character remains a mystery. Particles motivated by supersymmetry (Weakly Interacting Massive Particles (WIMPs)), extra dimensions (Kaluza Klein Particles), and a solution to the strong CP problem (the pseudoscalar axion), are among the best motivated from a particle physics standpoint (see [1, 2] for reviews). Experimental efforts searching for such elementary particle dark matter have focused on utilizing their strong or electroweak interactions to detect them, either directly through their interactions with ordinary matter, or indirectly through their annihilations to photons.

On another front, gravitational lensing has already proven an effective way to probe the nature of dark matter experimentally. Photometric monitoring of many stars has been used to search for gravitational lensing by lumps of dark matter, generically known as Massive Compact Halo Objects (MACHOs) [3, 4, 5, 6]. Dark matter dominated by compact objects such as baryonic planets, stellar remnants or black holes is now only allowed for $m_H \lesssim 10^{-7} M_\odot$ and $m_H \gtrsim 30 M_\odot$ [7]. However, there remains the “microlensing puzzle”, which is that MACHOs are observed and appear to contribute an optical depth toward the Large Magellenic Cloud (LMC) too large by a factor ~ 5 to be accounted for by simple models of the stellar population. Although the results are not consistent with all of the dark matter being in the form of MACHOs, their result [3] is consistent with an object of mass $M \sim 0.4 M_\odot$ accounting for 20% of the halo mass. This signal is also at variance with the EROS experiment results [6], which exclude $0.4 M_\odot$ MACHOs from composing more than 7% of the halo.

Searches for MACHO-like objects in the halo continue [6, 8], and in the future, lensing searches for objects on cosmological scales will be increasingly sensitive to objects in a wider range of masses (see [9, 10] for proposals on cosmological scale lensing using gamma-ray bursts, and [11, 12, 13, 14] for gravitational lensing from distant quasars). In addition, a large-aperture, wide-field spaceborne telescope is potentially capable of monitoring individual stars for lensing effects in a program similar to MACHO, but in galaxy halos orders of magnitude farther away than the current galactic lensing experiments (see [15] for lensing observations towards M87 in the Virgo cluster using the Hubble Telescope). In more distant halos, the Einstein radius for lensing by a given mass is considerably larger; therefore a wider range of objects can produce observable microlensing, and the probability of events increases.

The continued increasing capabilities in lensing experiments opens the possibility of detecting lensing variability from a wider class of astrophysical objects, beyond baryonic planets, stellar remnants and black holes, and has the potential for studying certain types of non-baryonic dark matter in detail. In particular, in this paper we study the effects of a type of non-baryonic, elementary particle dark matter that naturally forms into large, self-gravitating clumps in the early universe: scalar dark matter miniclusters. These structures originate from order unity isocurvature matter density fluctuations created during a second order phase transition of a very light scalar field, sometime after the QCD phase transition. The miniclusters form when these fluctuations subsequently collapse gravitationally at temperatures near matter-radiation equality.

It has been known for some time that the QCD phase transition gives rise to dense axion configurations, orig-

inally called miniclusters [16], or alternatively axitons [17, 18], with masses $M_{mc} \sim 10^{-12} M_\odot$, which are detectable by pico- or femto- lensing experiments [19]. The effects of large-scale modulation of axion density was also studied in [20, 21, 22]. We consider here a similar mechanism for a much wider class of theories, arising from a second order phase transition in either a Higgs-like or axion-like system, and with an associated phase transition temperature possibly much lower, perhaps even well below the QCD temperature. For this class of theories, the gravitational effects of the miniclusters are the main distinguishing effects of the character of the dark matter and the main experimental constraint on their parameters.

These scalar miniclusters (which we designate ScaMs for short) may be in a mass range interesting for lensing experiments. Although their densities are typically too low to be detectable by current generation galactic lensing experiments (and as a result, the MACHO dark matter constraints do not apply), they may be seen through longer baseline galactic lensing or cosmological scale lensing. As shown below, masses as large as $\sim 10^4 M_\odot$ are currently allowed without contradicting constraints on the power spectrum from the Ly α forest data. Other constraints on MACHO-like objects from tidal effects in halo wide binaries (as in [23]) also do not apply to ScaMs on account of the ScaMs' low internal densities. A significant fraction (as much as half) of the dark matter collapses into the compact objects initially, so it is natural to find significant microlensing rates under the right conditions. Unlike true MACHOs however, these objects are not point-like gravitational sources, but are extended objects with a radius which can be on the same order or larger than the Einstein radius, depending on the distance to the lens. This leads to the possibility of unique and distinctive gravitational lensing signatures. In the strong lensing regime, the ScaMs produce classical caustic events with sudden appearance and disappearance of images, associated with sudden large-amplitude variations in image brightness in variability surveys. In the weak lensing regime, sources passing behind a ScaM experience variable small-amplitude modulation depending on the projected surface density of the dark matter.

There are a wide range of theories which generate such objects. The second-order scalar field phase transition was introduced in ref. [24] within the context of axion cosmology to show that in the presence of late phase transitions the axion mass and coupling constant may lie outside the window prescribed by the conventional astrophysical and cosmological constraints; in particular a string scale axion with decay constant $f = 10^{16}$ GeV is allowed. In this model with a Higgs-like potential with a very small mass term, the field remains in the unbroken phase until the curvature of the potential is sufficiently large to overcome the Hubble friction, at which time the symmetry breaks as the field evolves to the minimum of the potential. Pseudo-Goldstone bosons have also been invoked for a variety of uses, the most famous of which

is the axion to solve the strong CP problem. They have been used in relation to attempts solve the cosmological constant problem [25], explain the origin of large-scale structure [26, 27], and provide a warm dark matter candidate [28]. The considerable increase in our knowledge of cosmological parameters has ruled out or disfavored a number of these scenarios, however the pseudo-goldstone boson remains a viable dark matter candidate.

The microlensing experiments have the capability of detecting these scalar objects which may never be observed directly through particle interactions due to their very weak couplings. The weak couplings are required by naturalness arguments. If there is no symmetry to protect their masses, radiative corrections tend to force scalars to be as heavy as the cut-off scale, which, for electroweak SUSY breaking, is $m_{susy} \sim 100$ GeV. In order to maintain a scalar as light as $\Lambda_{QCD}^2/M_{pl} \sim 10^{-21}$ GeV, this scalar must be protected from this SUSY breaking; this is done by requiring a small enough coupling to the visible sector that sufficiently small radiative corrections are generated for the light scalar field. We require in particular that its coupling λ to all ordinary matter satisfy $\lambda < m_\phi/m_{susy}$. Such an object is truly dark, undetectable even by the most sensitive particle dark matter detectors; like black holes, we can detect their presence only through their gravitational interactions.

In addition to lensing, these objects seed non-standard bottom-up hierarchical structure formation. The phase transition injects a large amount of fluctuation power on small scales so that nonlinear clusters are predicted already at recombination; they can accrete baryons, and potentially trigger star formation (possibly assisting early re-ionization), much earlier than the standard dark matter with only inflationary perturbations. This also implies that measurements of the matter power spectrum from the Lyman-Alpha forest will limit the masses of these objects; we derive constraints below.

The plan of the paper is as follows. In the next section we describe the physical dark matter models of interest, and derive general expressions for the density fluctuations. We then discuss the phenomenology of ScaMs, including the limits on their masses and radii from microlensing experiments and measurements of the power spectrum of the Lyman-Alpha forest. We use an N-body code to determine their density profiles, and consider their gravitational lensing effects in two regimes, strong and weak lensing, corresponding to distant and nearby halos respectively. We briefly discuss the evolution of these objects and their impact on structure formation, in particular early star formation. We close by surveying the viability of detecting and studying this dark matter candidate through its lensing effects.

II. SCAMS AND A LATE COSMOLOGICAL PHASE TRANSITION

A. Formation of isocurvature fluctuations

Consider the generic potential of a complex scalar field $\phi = \rho e^{ia/f}$,

$$V(\rho, a) = -m_\rho^2 \rho^2 + \lambda \rho^4 + \mu^4 \left(1 - \cos \frac{a}{f}\right) \quad (1)$$

Such a potential is similar to that generated for the QCD axion, the difference being that QCD instanton effects result in μ effectively being a time dependent quantity. That such a potential generates $\mathcal{O}(1)$ fluctuations in the resulting dark matter has been known for some time [16]. We review the basics here. If the Peccei-Quinn symmetry breaks after inflation has already occurred, it is expected that the initial value of the field will vary spatially, $-\pi \leq \theta \leq \pi$. As the QCD phase transition nears at $T \simeq 1$ GeV the axion gains a mass due to QCD instanton effects, generating a potential for the axion favoring $\theta = 0$. Initial spatial fluctuations in the field, θ_i , are then translated into spatial fluctuations in dark matter density, $\rho_{DM} \propto \theta_i^2$. As the fluctuations in θ_i are $\mathcal{O}(1)$, the axion dark matter fluctuations are also expected to be $\mathcal{O}(1)$. Thus the matter power spectrum enters matter-radiation equality already non-linear. These fluctuations immediately collapse at matter-radiation equality into dense objects, ScaMs. For the particular case of axions, the mass of these objects was shown to be approximately $10^{-12} M_\odot \sim \rho_a(T \simeq 1 \text{ GeV}) d_H^3$, the total dark matter mass within the horizon, d_H , at the time of the QCD phase transition.

These arguments carry over generally to any type of pseudo-Goldstone boson, provided, like the axion, the symmetry for the radial mode breaks after inflation, and the angular mode is effectively massless when this symmetry breaking occurs. Like the axion, a phase transition generates large density fluctuations, but we allow the transition to occur potentially much later, giving rise to more massive ScaMs. In the appendix we give an example of a specific supersymmetric model which gives rise to such late phase transitions. We call these pseudo-Goldstone boson modes axion-like modes on account of the similarity to the axion itself. These axion-like modes, however, need not be connected to QCD physics in any way.

In similar fashion, we may also consider Higgs-like modes. If the radial mode is sufficiently light, a Higgs-like potential may also generate a late second-order phase transition when ρ breaks the $U(1)$ symmetry. We will see that this second-order phase transition also results in $\mathcal{O}(1)$ density fluctuations in dark matter condensate. The radial field ρ remains in an unbroken phase at the origin, $\rho_i = 0$, until the curvature there exceeds the Hubble friction, $m_\rho > H$, when the field rolls out to its true minimum at $\langle \rho \rangle = f$. We will show that quantum fluctuations about ρ_i result in $\mathcal{O}(1)$ variations in the the

roll-off time of the scalar field. These $\mathcal{O}(1)$ variations in the roll-off time translate to $\mathcal{O}(1)$ variations in the density, due to spatial modulations in the temperature when the dark matter condensate forms and begins to redshift. In particular, we calculate

$$\frac{\delta \rho}{\bar{\rho}} = \frac{\bar{T}_{trans}^3}{T_{trans}^3} - 1, \quad (2)$$

where bars denote mean values, T_{trans} is the phase transition temperature in a particular Hubble patch, and

$$\bar{\rho}(T) = m_\rho^2 f^2 \left(\frac{T}{\bar{T}_{trans}} \right)^3. \quad (3)$$

It will be useful to rewrite this in terms of a time delay, δt from the mean time of the phase transition, \bar{t}_{trans} ,

$$\frac{\delta \rho(\mathbf{x})}{\bar{\rho}} = \left(\frac{t_{trans}(\mathbf{x})}{\bar{t}_{trans}} \right)^{3/2} - 1 = \left(1 + \frac{\delta t(\mathbf{x})}{\bar{t}} \right)^{3/2} - 1, \quad (4)$$

where we have included the explicit spatial dependence of $\delta \rho(\mathbf{x})$ on scales exceeding the Hubble size at the time of the phase transition. We can see that in the limit that $\delta t \lesssim \bar{t}$, the result reduces to

$$\frac{\delta \rho(\mathbf{x})}{\bar{\rho}} \simeq \frac{9}{2} H(\bar{T}_{trans}) \delta t(\mathbf{x}), \quad (5)$$

which is identical to the inflationary result for an upside-down harmonic oscillator [29], up to the multiplying factor.

As a result, in order to calculate the density fluctuations, we need only calculate the time delay. This is approximated by [29]

$$\delta t(\mathbf{x}) \simeq \lim_{t \rightarrow \infty} \frac{\delta \phi(\mathbf{x}, t)}{\dot{\phi}^{(0)}(\mathbf{x}, t)}, \quad (6)$$

where we have expanded in fluctuations, $\delta \phi(\mathbf{x}, t)$, around the background field, $\phi^{(0)}$, $\phi(\mathbf{x}, t) = \phi^{(0)}(t) + \delta \phi(\mathbf{x}, t)$.

We determine the classical evolution of the background field $\phi^{(0)}$ from its equation of motion,

$$\ddot{\phi}^{(0)}(t) + 3H\dot{\phi}^{(0)}(t) + m^2\phi^{(0)}(t) = 0. \quad (7)$$

Since we are interested in the behavior at asymptotically late times, we ignore the Hubble friction terms, and the solution is

$$\phi^{(0)}(t) = \phi_0^{(0)}(t=0)e^{mt}. \quad (8)$$

Likewise, we can determine $\delta \phi(\mathbf{x}, t)$ from an equation of motion

$$\ddot{\delta \phi}(\mathbf{x}, t) + 3H\dot{\delta \phi}(\mathbf{x}, t) + m^2\delta \phi(\mathbf{x}, t) - \nabla^2\delta \phi(\mathbf{x}, t) = 0. \quad (9)$$

For large times, we may neglect the spatial gradient and Hubble friction terms, and the solution is

$$\delta \phi(\mathbf{x}, t) = \delta \phi(\mathbf{x}, t=0)e^{mt}. \quad (10)$$

Thus $\delta t(\mathbf{x})$ is set entirely by initial conditions:

$$\delta t(\mathbf{x}) \simeq \frac{\delta\phi(\mathbf{x}, t=0)}{\phi^{(0)}(t=0)} \frac{1}{m}. \quad (11)$$

We will assume that the background field $\phi^{(0)}$ is initially at the origin. However, we cannot choose $\phi^{(0)}(t=0) = 0$ because of quantum fluctuations. The size of these fluctuations are calculated from the Fourier transform of the two point function, following [29]:

$$\begin{aligned} \Delta\phi(\mathbf{k}) &\equiv \left[\frac{k^3}{(2\pi)^3} \int \frac{d^3x}{(2\pi)^3} e^{i\mathbf{k}\cdot\mathbf{x}} \langle \delta\phi(\mathbf{x}, t=0) \delta\phi(0) \rangle \right]^{1/2} \\ &= \left[k^3 \int \frac{d^3k'}{(2\pi)^3} \int \frac{d^3x}{(2\pi)^3} e^{i\mathbf{k}\cdot\mathbf{x}} e^{i\mathbf{k}'\cdot\mathbf{x}} \right]^{1/2} \\ &= \frac{k}{(32\pi^3)^{1/2}} \end{aligned} \quad (12)$$

For the mode of interest, $k = m$, these fluctuations set both $\phi^{(0)}(t=0)$ and the root mean square (rms) value of $\delta\phi(\mathbf{k})$, the Fourier transform of $\delta\phi(\mathbf{x}, t=0)$. Putting it all together, we have the rms density fluctuations,

$$\begin{aligned} \frac{\Delta\rho_{rms}}{\bar{\rho}} &\simeq \frac{9}{2} \frac{\Delta\phi(k=m)}{\phi^{(0)}(t=0)} \frac{H(\bar{T}_{trans})}{m} \\ &\simeq \frac{1}{2\sqrt{2}}, \end{aligned} \quad (13)$$

showing that the density fluctuations are of order unity.

B. ScaM collapse

These fluctuations collapse gravitationally into ScaMs around the time of matter-radiation equality. For collapse of a uniform sphere the final core density of a virialized ScaM is [18]

$$\rho = 140\delta^3(\delta+1)\rho_{eq}, \quad (14)$$

where $\delta = \delta\rho/\bar{\rho}$. Their masses are set by the dark matter mass inside the horizon at the time of the phase transition,

$$M_{ScaM} = \frac{4}{3}\pi d_H^3 \rho_{DM}(T_{trans}), \quad (15)$$

where $d_H = H(T_{trans})^{-1}$. This corresponds to a ScaM mass, assuming these scalars compose a fraction r of the dark matter,

$$M_{ScaM} \simeq 1.4 \times 10^{-3} M_\odot r \left(\frac{10^{-3} \text{ GeV}}{T_{trans}} \right)^3. \quad (16)$$

C. Limits on ScaM Mass from Lyman- α

As a result of these non-linear density fluctuations, the phase transition adds a large amount of fluctuation power into the spectrum on small scales. These

scales, $r_s \sim T_{trans}/(T_0 H(T_{trans}))$ (~ 10 pc (comoving) for $T_{trans} \sim \Lambda_{QCD}$) are well below the reach of current measurements of the power spectrum, since the smallest scale measurements, derived from observations of the Lyman- α absorption of the spectra of distant quasars [30, 31, 32], reach down only to scales $\sim 0.1h^{-1}$ Mpc, the scale where protogalactic gas is collapsing into mildly nonlinear filaments. The phase transition, however, generates a Poisson white noise power spectrum on scales larger than r_s which adds to the inflationary power on the Lyman- α scale,

$$P_p = \frac{1}{n_{ScaM}}, \quad (17)$$

where n_{ScaM} is the number density of ScaMs and the subscript p is for primordial. The added power today is then the product of the primordial white noise power spectrum with the transfer function for isocurvature fluctuations, T_{iso} ,

$$P_{wn} = T_{iso}^2 P_p, \quad (18)$$

where

$$T_{iso} = \frac{3}{2}(1+z_{eq}). \quad (19)$$

Now neither P_p nor T_{iso} is wave number k dependent, whereas P_{CDM} decreases with k . We plot this power spectrum in fig. 1. We have introduced in the white noise spectrum a smoothing scale $r_s \simeq d_H(T_{trans})$, on which the Kibble mechanism smooths field fluctuations, to remove power on the smallest scales,

$$P_{ScaM} = P_{wn} e^{-(kr_s/2\pi)^2/2}. \quad (20)$$

We can see from fig. 1 that for sufficiently large k , P_{ScaM} will exceed P_{CDM} ; we must ensure that this occurs on smaller scales than are reachable with Lyman-alpha measurements, $k > k_J$, so that we require

$$\frac{9}{4}(1+z_{eq})^2 \frac{M_{ScaM}}{\rho_{DM}} < P_{Ly\alpha}(k_J), \quad (21)$$

where $k_J \simeq 10h$ Mpc $^{-1}$. This yields the constraint

$$M_{ScaM} \lesssim 4 \times 10^3 M_\odot, \quad (22)$$

corresponding to a constraint on the temperature of the phase transition,

$$2 \times 10^{-5} \text{ GeV} \lesssim T_{trans}, \quad (23)$$

assuming the scalars compose all the dark matter. A similar constraint from the Lyman-alpha power spectrum was derived in [33] using numerical simulations in the context of primordial black holes.

Phase transitions between the QCD scale and this Lyman- α limit create abundant ScaMs in the mass range

$$10^{-12} M_\odot \lesssim M_{ScaM} \lesssim 4 \times 10^3 M_\odot, \quad (24)$$

much of which is accessible to current and future microlensing experiments.

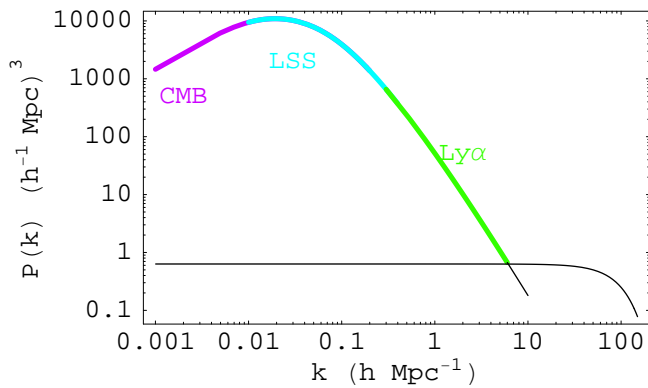


FIG. 1: CDM power spectrum derived from BBKS [34] with white noise power spectrum smoothed on scales $r_s \simeq 7 \times 10^{-2}$ Mpc, given by eqn. 20. The amplitude of the white noise spectrum corresponds to the power spectrum for a ScaM of mass $M \simeq 4 \times 10^3 M_\odot$.

D. ScaMs as microlenses

For ScaMs to act as observable strong microlenses, three conditions must be satisfied:

1. ScaM masses must lie in the mass range reachable by experiments. For classic microlens searches by stellar monitoring in the local halo, this range is currently $10^{-7} M_\odot \lesssim M_{ScaM} \lesssim 10 M_\odot$. However, the accessible range will widen in the future as microlensing experiments access fainter and more distant monitored background sources in other galaxies.
2. A rough criterion for strong lensing, leading potentially to large-amplitude variations in source brightness, is that the radius of the ScaM be smaller than the Einstein ring radius. For microlensing of objects over cosmological distances, the Einstein radius is

$$R_E \simeq 3 \times 10^{16} \left(\frac{M}{1 M_\odot} \right)^{1/2} \text{ cm.} \quad (25)$$

For lensing toward a source in the local galactic neighborhood (e.g. toward the LMC or M31), the Einstein Radius is

$$R_E \simeq 3 \times 10^{14} \left(\frac{M}{1 M_\odot} \right)^{1/2} \left(\frac{D}{50 \text{ kpc}} \right)^{1/2} \text{ cm,} \quad (26)$$

where D is the distance to the lens, and it is assumed that $D \ll D_s$, the distance to the source.

Using the spherical model, eqn. 14, and assuming that the ScaMs are approximately constant density, we calculate

$$R_{ScaM} = 4 \times 10^{16} \frac{1}{\delta ((\delta + 1) \Omega_\phi)^{1/3}} \left(\frac{M_{ScaM}}{1 M_\odot} \right)^{1/3} \text{ cm.} \quad (27)$$

3. Their cosmological abundance must be consistent with the limits from the current lensing experiments. Since these objects would generally be too fluffy to create strong lensing in the nearby halos observed by the current generation of galactic microlensing experiments, consistency with the limits of these experiments is generally not problematic.

Although these objects would generally not be dense enough to be observed by Galactic microlensing experiments, they may be detectable as microlenses for more distant sources and halos. If they do produce strong lensing events, they do not obey the classic Paczynski [35] point-mass light curve, but instead are dominated by more generic caustic-crossing events. More generally, in nearby halos they may not even act as strong lenses, but may have a resolved density structure that appears as small-amplitude variations in the light curve of a lensed source.

To improve on the spherical collapse model, eqn. 14, and in particular to determine properties of these objects observable by lensing experiments, we simulate the collapse of ScaMs using an N-body code. The resulting objects are more realistic than the spherical model and allow determination of some representative density profiles.

III. SIMULATING SCAMS

We simulate the formation of ScaMs in the radiation dominated era using the N-body code described in [36].

A. Initial conditions

The initial density profile may be determined utilizing one of two methods: either by solving the classical equations of motion for a field ϕ directly, or simply using the power spectrum of eqn. 17. The equation of motion for a scalar field is given simply by

$$\ddot{\phi} + 3H\dot{\phi} - \frac{1}{R^2(t)} \nabla^2 \phi + \frac{\partial V(\phi)}{\partial \phi} = 0, \quad (28)$$

where the Laplacian is taken with respect to comoving coordinates x . We can rewrite this (see [18] for details) in terms of conformal time, $\eta \equiv R/R_1$, where R_1 is defined by $H(R_1) = m_\phi$, and comoving Laplacian $\bar{\nabla}^2$, taken with respect to coordinates $\bar{x} = H(R_1)R_1 x$,

$$\phi'' + \frac{2}{\eta} \phi' - \bar{\nabla}^2 \phi + \frac{\eta^2}{m_\phi^2} \frac{\partial V(\phi)}{\partial \phi} = 0. \quad (29)$$

We assume the system is subject to white noise initial conditions,

$$\phi_i = A \sum \frac{\sin(\omega\eta)}{\omega\eta} \sin(p_i x + \xi_{1ijk}) \sin(p_j y + \xi_{2ijk}) \times \sin(p_k z + \xi_{3ijk}), \quad (30)$$

where the ξ 's are random phases.

We solve the equation of motion on a lattice 100 sites per side for the axion-like potential, $V(\phi) = 1 - \cos(\phi/f) = 1 - \cos\theta$. This potential would result in the formation of domain walls if, for example, $A = \pi f$ (in the language of axions, this corresponds to multiple vacua, $N > 1$). The walls are transient objects that quickly dissipate by particle radiation, but introduce singularities that make numerical integration difficult. Since we are interested in the formation and evolution of the ScaMs only, we avoid this problem by choosing A so that θ varies between $-\pi$ and π , and the root-mean square (rms) value of $\theta_i = \phi_i/f$ is the rms average value of the misalignment angle, $\theta_{rms} = \pi/\sqrt{3}$. In this case, the domain walls never form in our box.

Solving the equation of motion numerically automatically simulates the effects of the Kibble mechanism, smoothing field fluctuations on scales smaller than the horizon size at the time of the phase transition. We plot in fig. 2 a two dimensional slice of the initial white noise density fluctuations for the axion-like potential.

We evolve these fluctuations to $\eta = 10$, at which point the fluctuations are expected to remain mostly spatially frozen (modulo logarithmic growth of fluctuations) until gravitational collapse begins right around (or even somewhat before for the most dense ScaMs) the epoch of matter-radiation equality. The density fluctuations in a box with sides whose length are four times the horizon size at the time of the phase transition are shown in fig. 3. The density fluctuations have been normalized to the average density in the box, so that $\rho(\mathbf{x})/\bar{\rho}$ is shown.

We choose an alternate method to determine initial density fluctuations for the Higgs-like potential. According to eqn. 13, the Higgs-like potential gives only quasi-nonlinear density perturbations, which allows us to model the formation of these clumps realizing the initial density fluctuations using the standard N-body particle method: particles are initially placed on a lattice to minimize shot noise, then displaced from those positions by adding perturbations, mode by mode in the Zel'dovich approximation, with amplitudes and phases selected according to the distribution derived from the power spectrum. We adopt the power spectrum of eqn. 20

$$P(k) = Ae^{-(kr_s/2\pi)^2/2} \text{Mpc}^3, \quad (31)$$

which creates white noise filtered on a scale r_s . This smoothing scale corresponds roughly to the horizon size at the time of the phase transition. The expected density fluctuations on this scale are thus

$$\left(\frac{\delta\rho}{\rho}\right)_{rms}^2 = \frac{9}{2\pi^2} k_s^2 \int_0^\infty P(k) \left(\frac{\sin(k/k_s)}{(k/k_s)^2} - \frac{\cos(k/k_s)}{kk_s}\right)^2 dk, \quad (32)$$

where $k_s = 2\pi/r_s$ and we choose r_s so that the resulting ScaMs has masses around $1M_\odot$ (calculated from $M_{ScaM} \sim \rho_{DM} r_s^3$, and corresponding to a phase transition temperature, $T_{trans} \sim 10^{-4}$ GeV), and A such that

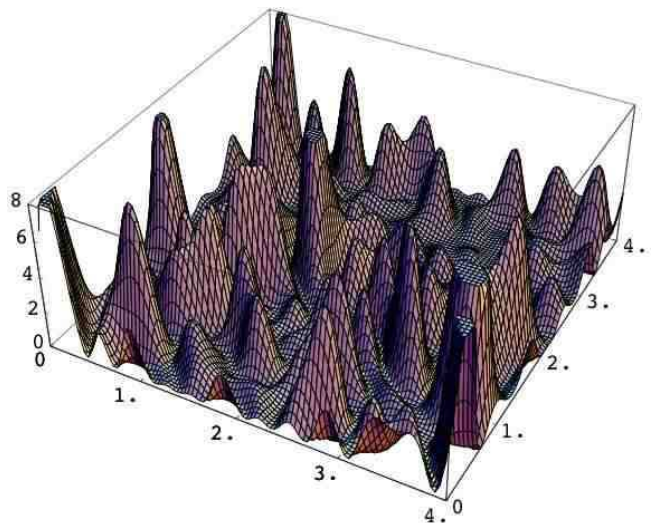


FIG. 2: Two-dimensional slice in the x-y plane of initial white noise field energy density distribution. x-y coordinates are in η , where $\eta = 1$ corresponds to a length $d_H(T_{trans})$, one horizon size at the time of the phase transition. The z-axis is the initial white noise over-density $\rho(\mathbf{x})/\bar{\rho}$, where $\bar{\rho}$ is the mean density in the box.

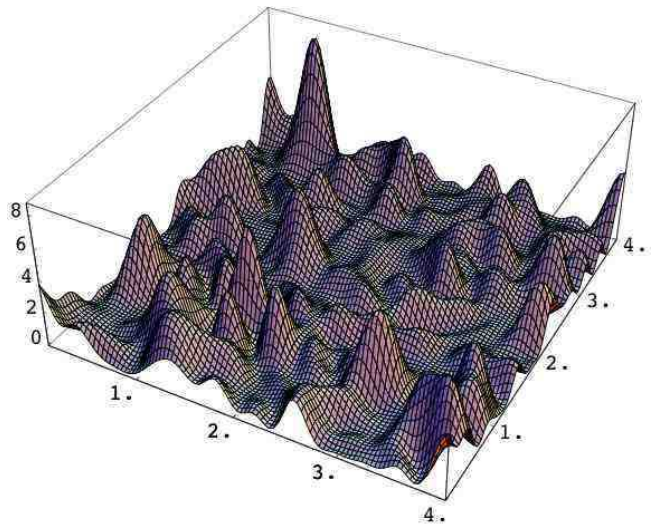


FIG. 3: Density distribution after the phase transition, at $\eta = 10$ for the axion-like potential. Axes are same as in fig. 2. Note the highly nonlinear nature of the initial density perturbations. This distribution remains fixed until near matter-radiation equality when it evolves gravitationally into collapsed ScaMs; this density spectrum is the input for the N-body simulation.

$(\delta\rho/\rho)_{rms} \simeq 0.5$. Note that while we use specific physical scales for the purpose of the simulation, the result is expected to be completely scale invariant, and should apply with suitable rescaling to ScaMs of all masses.

We plot the corresponding density fluctuations for the Higgs-like potential in fig. 4. We then use the N-body code to evolve the objects into the collapse epoch near

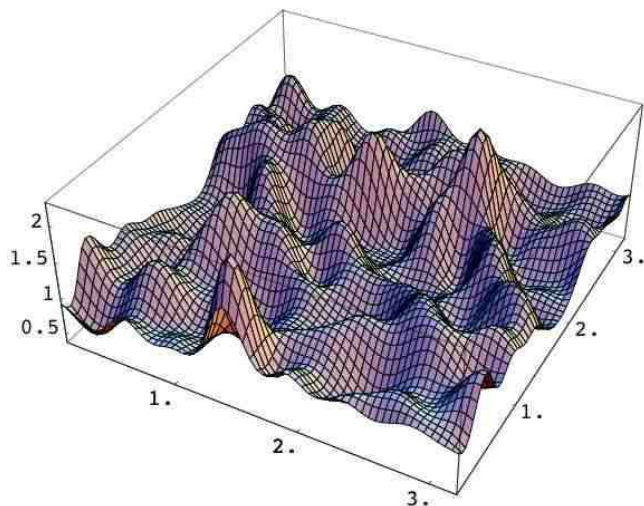


FIG. 4: Density distribution generated by the smoothed white noise power spectrum. The size of the density fluctuations were chosen consistent with the analytic result for the Higgs-like potential of Sec. II. Like fig. 3, this distribution is input for the N-body simulation.

matter-radiation equality.

B. N-body simulation of ScaM density profiles

Using the density profile generated by solving the classical equations of motion for the axion-like potential, a grid of 100^3 particles is laid with masses weighted according to the locally computed initial density. The evolution of the particles is started at a redshift 1×10^5 ; objects are fully collapsed by matter radiation equality, around a redshift of 3000. As the density fluctuations are initially much smaller for the Higgs-like distribution shown in fig. 4, the evolution can be started much later; we choose a redshift of 1×10^4 , and objects are fully collapsed by a redshift of 1000.

We show in figs. 5, 6 a slice of the final particle distributions of the collapsed objects, at redshifts around matter radiation equality. The initial over-densities shown in figs. 3, 4 evolve into the fully collapsed objects shown in figs. 5, 6. The pictures of course resemble images of the low-redshift cosmic web of dark matter, but in this case represent very small-scale, nonlinear objects at a redshift around 10^3 . The “normal” inflationary perturbations in dark matter at this time still have a very small amplitude on all scales, of the order of one percent.

We plot in figs. 7, 8 the density profiles of a sampling of ScaMs, where we choose to normalize our densities and radii against those predicted by the spherical model, eqn. 14, for $\delta = 1$. We can see that the naive spherical model is approximately accurate in predicting the maximum density of the ScaMs. The axion-like potential has typical overdensities $\delta \sim 5 - 10$, as shown in fig. 3, so that

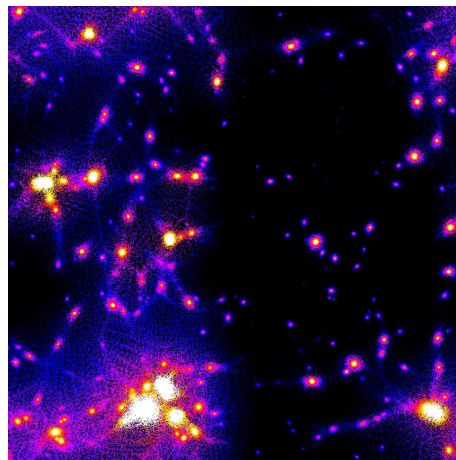


FIG. 5: Snapshot of structure formation at $z = 3000$ for axion-like ScaMs; the plot is colored according to the logarithm of the density. The scale here is $1.2h^{-1}$ Mpc, in co-moving coordinates, although the result is expected to be invariant for any box size, given that we rescale the smoothing scale accordingly. Note that structure formation has already commenced before matter radiation equality.

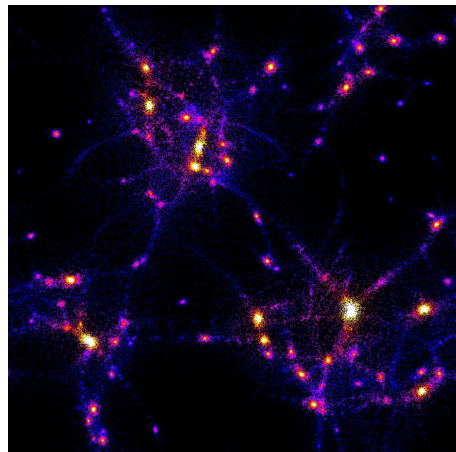


FIG. 6: Same as fig. 5, but for the Higgs-like potential at a redshift $z = 1000$. This simulation was evolved to a lower redshift, as the initial over-density of the Higgs-like system is lower, and hence gravitational collapse occurs later. Although difficult to see from this rendering, the densities of the ScaMs are also lower.

the spherical model predicts $\rho/\rho_{sph}(\delta = 1) \sim 100 - 5000$. The Higgs-like potential, on the other hand, has typical overdensities $\delta \sim 0.5 - 1$ (fig. 4), and so we expect $\rho/\rho_{sph}(\delta = 1) \sim 0.1 - 1$, again consistent with the central densities given by the simulation. The ScaMs with higher central densities correspond to ScaMs which had higher initial overdensity δ .

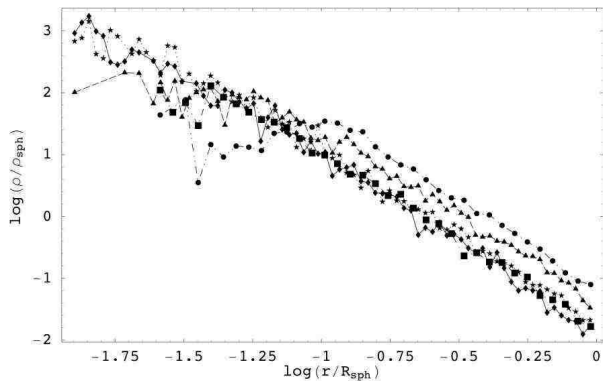


FIG. 7: Axion-like ScaM density profiles for five gravitationally collapsed ScaMs. Vertical axis is $\log(\rho(r)/\rho_{sph})$, where $\rho_{sph}(\delta = 1) = 280\rho_{eq}$; that is, we normalized the density profile against the uniform density prediction of the spherical model, eqn. 14, with $\delta = 1$. Horizontal axis is $\log(r/R_{sph})$, where R_{sph} is the radius computed from ρ_{sph} and the total mass contained within the horizon at the phase transition, $d_H(T_{trans})$.

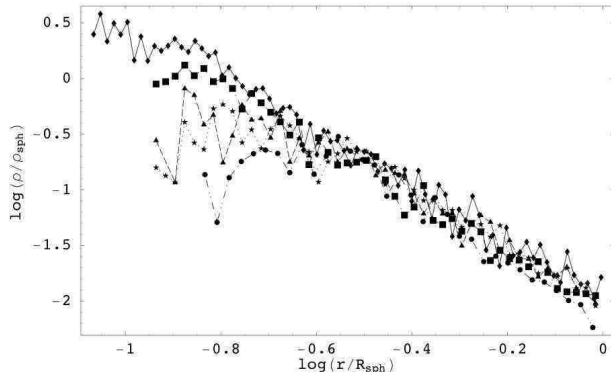


FIG. 8: Same as fig. 7, but for the Higgs-like potential.

C. Strong lensing profiles

What is the implication for lensing experiments? As explained in section III, in order for an object to act as a strong gravitational lens, the enclosed mass, M_{encl} , at any given radius must exceed a minimum,

$$M_{encl}(r) > 1M_{\odot} \left(\frac{r}{s(D)} \right), \quad (33)$$

where $s(D)$ is dependent on the base length for lensing, D ($s \sim 3 \times 10^{15}$ cm for $D = 5$ Mpc, and $s \sim 3 \times 10^{14}$ cm for cosmological scale lensing). Equivalently, at any given distance from the center of the object r , the radius must not exceed the Einstein radius,

$$r < R_E = s(D) \left(\frac{M_{encl}}{1M_{\odot}} \right)^{1/2}. \quad (34)$$

The Einstein radius can be computed directly from density profiles shown in figs. 7, 8.

We plot in figs. 9, 10 R_E versus r , for $s = 3 \times 10^{15}$ cm, 3×10^{14} cm. As in figs. 7, 8, we have normalized the radii against R_{sph} , the prediction of the spherical model. The objects lens if $R_E > r$, that is, if the Einstein profiles lie above the straight line, $R_E = r$, shown in the figure. Although the simulation was run for a particular mass within the horizon at the time of the phase transition, $M \sim 1M_{\odot}$, it is simple to apply the results to many different ScaM masses simply by rescaling the total mass in the box. In this scaling R_E increases like $M^{1/2}$, but the box size decreases like $M^{1/3}$ so the net result is that the vertical axis in the figure is scaled up by $M^{1/6}$, meaning that more massive ScaMs lens more easily. Note that the mass labeled is the mass enclosed within the horizon at the time of the phase transition, not the lensed mass of the ScaM, which may be significantly lower.

We can see that both Higgs-like and axion-like ScaMs are of interest for lensing experiments on a cosmological scale, from objects as light as $10^{-6}M_{\odot}$ to as heavy as the cosmological bound of $4 \times 10^3M_{\odot}$. While neither of these objects is of interest for the current galactic lensing experiments with baseline $D \sim 50$ kpc, the axion-like configuration in particular will be of interest for lensing in the Mpc range and greater, as might be accessible in future experiments. We also note here that we have not chosen the most extreme set of initial conditions to simulate for the axion-like potential. The axion itself has a time dependent mass around the time of the phase transition which results in larger density contrast. Normalizing against the size of the box, we find that axions in particular generate overdensities $\delta \sim 20 - 30$. (Kolb and Tkachev [18] found larger overdensities $\delta \sim 30 - 100$ as they normalized against the density for $\theta_{rms} = \pi/\sqrt{3}$ and not the actual average density in the box.) In this case, R_E for the axion-like potential is increased by as much as a factor of 10, which improves the observational prospects.

As long as the radius of the lens is much bigger than the size of the background source, those situations where $R_E > r$ will occasionally lead to strong-lensing events with high amplification. The frequency of this happening is roughly given by the fraction of the halo mass in ScaMs above this threshold, times the mean lensing optical depth of the halo, times A^{-2} where A is the amplification. The mean optical depth is a very small for nearby halos ($\approx 10^{-6}$ for the LMC experiments) but is typically ≈ 0.1 for halos at cosmological distances. Such considerations affect the number of sources and the cadence of observations needed in a variability survey.

D. Weak lensing: mapping ScaMs using variability

Even if ScaMs are not dense enough to cause strong-lensing events, they can in general still produce weak lens amplification. In some situations the systems are small enough that this amplification is time variable, and the projected density profiles of ScaMs can be measured

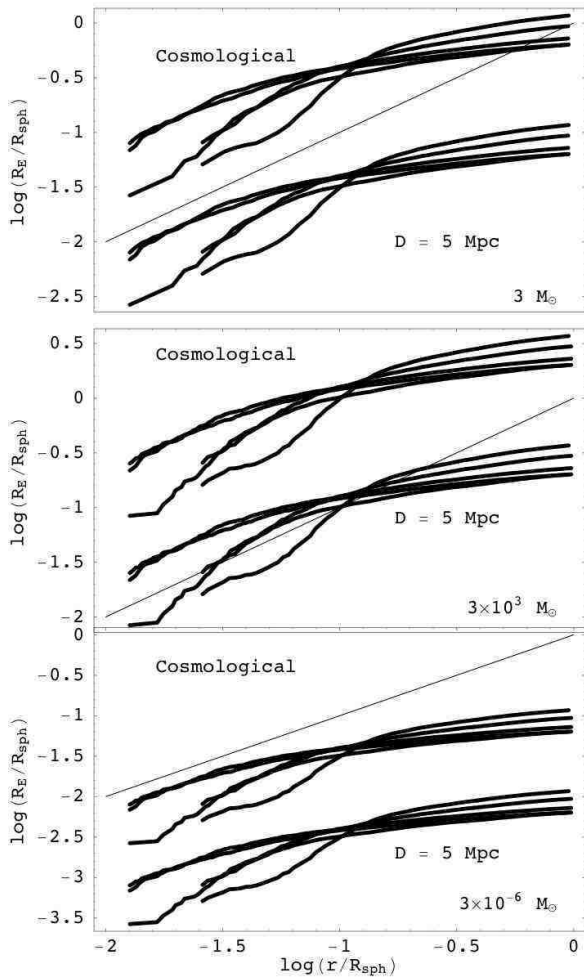


FIG. 9: Axion-like ScaM Einstein radius for the enclosed mass, derived from the computed N-body density profile, versus ScaM radius, again normalized against the ScaM radius R_{sph} predicted by the spherical model. The diagonal line divides where $R_E > r$, when lensing is possible. The upper set of curves in each plot is the Einstein radius for cosmological scale lensing, the lower set of curves the Einstein radius for lensing at a distance $D = 5$ Mpc, which may be relevant for MACHO-type experiments in nearby galaxy halos. This is shown for three different ScaM masses, marked at the lower right in each plot.

directly by monitoring sources. Survey parameters, such as the distance of the halo under study and the number of sources to be monitored, can be optimized depending on the predicted ScaM parameters; in principle, both weak and strong lensing can be studied at various distances.

Consider a standard gravitational lens mapping a source at position $\vec{\theta}_S$ in the source plane to a position $\vec{\theta}_I$ in the image plane. In the image plane the mapping is characterized by the convergence κ and complex shear γ . The magnification μ is the inverse Jacobian of the

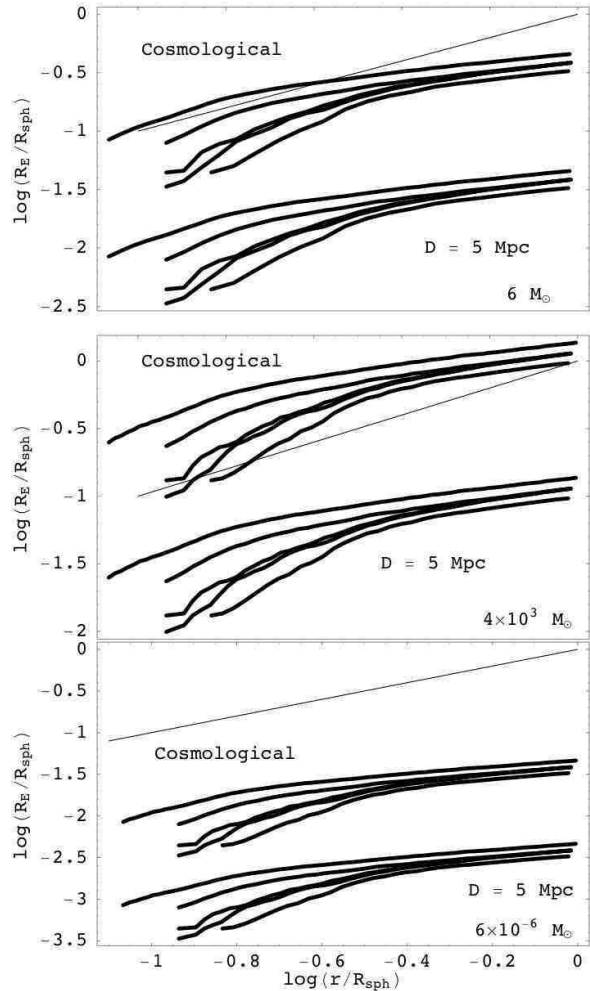


FIG. 10: Same as fig. 9, but for the Higgs-like potential.

mapping [37]

$$\mu^{-1} = (1 - \kappa)^2 - |\gamma|^2. \quad (35)$$

The convergence is determined by the surface density Σ along the line of sight,

$$\kappa = \Sigma / \Sigma_C, \quad (36)$$

where the critical surface density depends on the (angular diameter) distances to the source (D_S), the lens (D_L), and between them (D_{LS}) as:

$$\Sigma_C = D_{LS} c^2 / 4\pi G D_L D_S \approx 3.5 \text{ kg m}^{-2} (D_{LS} \text{ Gpc} / D_L D_S). \quad (37)$$

If $\Sigma > \Sigma_C$, generally light rays focus to a point somewhere, the mapping involves multiple images and generally strong shear, and amplification is both nonlocal and nonlinear. High-amplitude variability is in the strong lensing regime and dominated by caustics near fold catastrophes in the mapping. By contrast, in the case of weak

lensing, $\Sigma < \Sigma_C$, the amplification of a source is more directly related to the surface density in that direction. For small surface densities, and where the shear is negligible, the magnification is just

$$\mu = \left| \frac{\partial \vec{\theta}_S}{\partial \vec{\theta}_I} \right|^{-1} \simeq 1 + 2\kappa. \quad (38)$$

Thus as a source traverses behind a ScaM and Σ varies, its brightness changes by a fraction $2\Sigma/\Sigma_C$. We plot in figs. 11, 12 Σ/Σ_C for the axion-like and Higgs-like potentials. We see that the variability will be difficult to detect for the current lensing experiments towards the LMC and M31, as the effect is only a few percent even for the most massive ScaMs. The weak lensing variability, however, will be of interest for longer baseline experiments, $D = 5$ Mpc, and also for cosmological scale lensing. For an axion-like ScaM of mass $1M_\odot$, the time scale for variability is on the order of a year (assuming a ScaM velocity across the source of 300 km/s), and decreases with ScaM mass as $M_{ScaM}^{1/2}$.

Note that the weak lens effects cover more area, and have a larger probability of affecting a background source than the strong lens effects. For a given mass of lensing material, the lensing probability or optical depth scales in the weak regime like $\tau \propto \Sigma^{-1} \propto (\mu - 1)^{-1}$, but the distribution of mass in the outer parts of ScaMs is even more favorable to the weak lensing program. In the examples shown in figures 11 and 12, we see that variability at the ten percent level (that is, $\Sigma/\Sigma_C \approx 0.05$) occurs at a radius which is typically more than ten times the radius of strong lensing, so variation of this magnitude is over 100 times more frequent than strong lensing events. Photometric accuracy and stability are the main practical limits in mounting variability surveys around this effect, but long term variations at the few percent level are certainly within the range of proposed instruments (such as JDEM) designed to monitor distant supernovae.

IV. EARLY BARYON COLLAPSE

With WIMP-type dark matter such as neutralinos, inflationary fluctuations lead to collapse of the first dark matter halos of roughly an earth mass scale, determined by the damping scale of the WIMP streaming motions [38]. The collapse begins on after a redshift of 100 and on small scales has little effect on the baryons, since the gravitational potentials are so shallow.

With ScaMs on the other hand, the addition of isocurvature fluctuations creates deeper dark matter potentials at earlier times. We have already seen that the accretion of absorbing gas, leading to Ly α absorption, is indeed the main astrophysical constraint at present on ScaM mass. In this section, we estimate the nonlinear effects of ScaMs on early structure, using an analytic Press-Schechter approach to bottom-up hierarchical clustering.

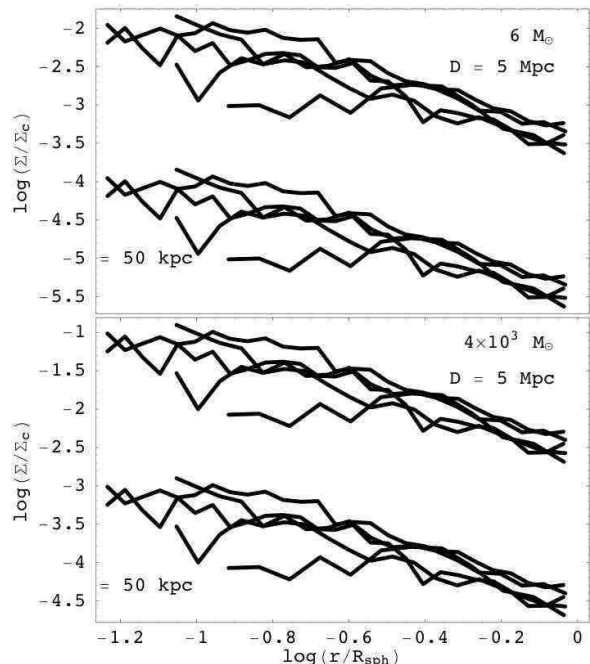


FIG. 11: Log mean surface density Σ relative to the critical density Σ_c as a function of log radius, averaged in annuli, normalized again to the prediction of the spherical model, R_{sph} . $\Sigma/\Sigma_c \sim 1$ corresponds roughly to the onset of strong lensing, and $2\Sigma/\Sigma_c$ corresponds to the fractional weak-lens amplification. Higgs-like potential.

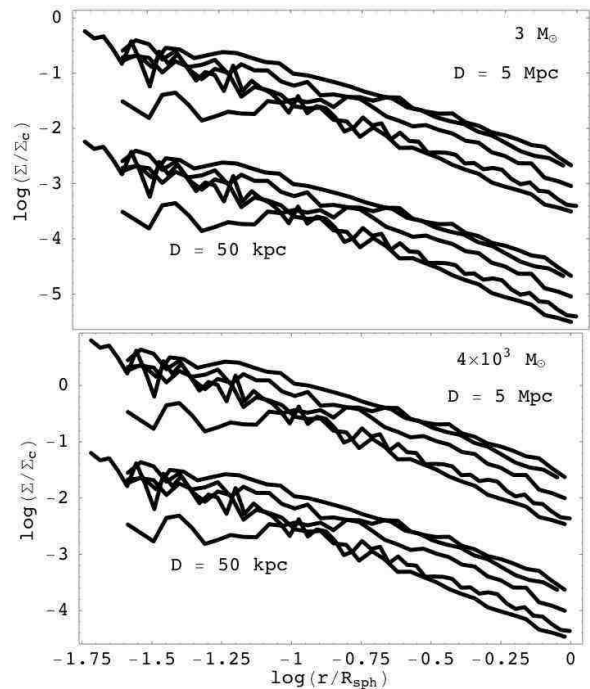


FIG. 12: Same as fig. 11, but for the axion-like potential.

Once the ScaMs form at $z_{eq} \approx 3300$, bottom-up hierarchical structure formation begins. In the spherical model, fluctuations on a scale M collapse into structures once the fluctuation has grown to a size

$$\delta(M) \simeq 1.69. \quad (39)$$

As the fluctuations are isocurvature, they grow as

$$\delta(M) = \delta(M_{ScaM}) \sqrt{\frac{M_{ScaM}}{M}} \frac{3}{2} \frac{1+z_{eq}}{1+z}, \quad (40)$$

where $\delta(M_{ScaM}) \simeq 1$. Therefore a structure of mass M will form at a redshift z_f

$$1+z_f \simeq \frac{1}{\delta(M)} \sqrt{\frac{M_{ScaM}}{M}} \frac{3}{2} (1+z_{eq}). \quad (41)$$

By making use of the spherical approximation, $\rho_M = 140\delta(M)_i^3(\delta(M)_i + 1)\rho_{eq}$, where

$$\delta(M)_i = \delta(M_{ScaM}) \sqrt{\frac{M_{ScaM}}{M}} \quad (42)$$

we also determine the virial radius of a structure of mass M ,

$$R(M) \simeq \left(\frac{M}{6 \times 10^2 \delta(M_{ScaM}) \rho_{eq}} \right)^{1/3} \sqrt{\frac{M}{M_{ScaM}}}, \quad (43)$$

and hence the virial velocity of these structures is

$$\begin{aligned} \sqrt{GM/R} &\simeq G^{1/2} (6 \times 10^2 \delta(M_{ScaM}) \rho_{eq})^{1/6} (MM_{ScaM}^3)^{1/12} \\ &\simeq 5 \times 10^{-6} \left(\frac{M}{1M_\odot} \right)^{1/12} \left(\frac{M_{ScaM}}{1M_\odot} \right)^{1/4}. \end{aligned} \quad (44)$$

If the baryons have a thermal velocity greater than the virial velocity, they are prevented by pressure gradients from collapsing into the ScaM. To trigger accretion and collapse we require the ScaM to have a virial temperature greater than that of the microwave background, since the baryons can certainly not radiate binding energy if they are cooler than that. The velocity of the baryons at the CMB temperature today would be $v \simeq \sqrt{3T_0/m_p} \simeq 9 \times 10^{-7}$. The baryons begin accretion onto the ScaM seeded structures once the velocity of the baryons drops below the structures' virial velocity, which occurs at redshift, z_{acc} ,

$$\begin{aligned} 2 \times 10^{-6} \left(\frac{M_{ScaM}}{1M_\odot} \right)^{1/3} \left(\frac{3}{2\delta(M)} \frac{(1+z_{eq})}{(1+z_{acc})} \right)^{1/6} \\ \simeq \sqrt{\frac{3T_0(1+z_{acc})}{m_p}}. \end{aligned} \quad (45)$$

Solving this, we find that baryon accretion onto the structures formed hierarchically from a ScaM seed of mass M_{ScaM} , occurs at a redshift

$$1+z_{acc} \simeq 30 \left(\frac{M_{ScaM}}{1M_\odot} \right)^{1/2}, \quad (46)$$

onto a structure of mass

$$M = \frac{1M_\odot}{\delta(M)^2} \left(\frac{1+z_{eq}}{1+z_{acc}} \right)^2. \quad (47)$$

We do not pursue further here the physics of the accreted baryons, which depends on complex details of non-linear collapse and cooling [39, 40, 41, 42]. However it is clear that the early star formation in the ScaM models can start much earlier than in standard CDM cosmology where significant collapses occur at a redshift less than about 30. With massive ScaMs, collapse can occur as early as recombination. Since cooling is relatively efficient at such early times (for example, through Compton cooling on the microwave background), these models also likely produce very early stars. These effects may eventually be observable either directly via deep infrared imaging, or indirectly via reionization effects. In any case it is clear that there would be significant modifications to early star formation with standard CDM perturbations.

V. CONCLUSION

We have not attempted to trace the evolution of the ScaMs in detail to the present, where they would be incorporated hierarchically into the standard galaxy-size dark matter halos. Although they would be subject to some disruption in the course of hierarchical assembly, there is good reason to think that they would mostly survive intact to the present. Certainly they fare better than the much more diffuse earth-mass halos of neutralino CDM [38]. In that case, the very flat distribution of density leads to a large range of masses collapsing almost at the same time on top of each other. Early ScaMs cluster instead with a steep white-noise spectrum, where the mass scale grows as a power law. In that situation there is more room for survival and less chance for disruption; the process of early ScaM clustering has a similar spectrum to, and therefore resembles, the larger galaxy-scale hierarchy today, where simulations have established that much of the satellite substructure survives. The clumpiness of dark matter in the halo may also have observable consequences through tidal forces, such as disruption of globular clusters; these effects have been studied in the context of black hole dark matter and other highly compact objects [43, 44, 45].

We have shown that in scalar theories with a cosmological phase transition below the QCD scale, ScaMs form with a mass in an interesting range for microlensing experiments, $10^{-12}M_\odot \lesssim M_{ScaM} \lesssim 10^4M_\odot$. The radii and density profiles of the ScaMs vary considerably, depending on the initial size of the density fluctuations. For an overdensity $\delta \sim 50$ and mass $M \sim 1M_\odot$, these objects would be visible for current galactic scale lensing experiments. Objects with (more plausible) lower overdensities $\delta \sim 5 - 10$, while not detectable with the current generation of experiments, would be visible for future lensing experiments with longer baselines, $D \sim 5$ Mpc or greater,

requiring a space based platform (or wide field adaptive optics) to conduct a lens-induced-variability survey. Cosmological scale lensing is the most powerful tool of all for detecting these objects, but on that scale, detailed monitoring studies are still in the distant future. Some information might be obtained sooner from quasar microlensing, but ScaMs tend to be not much larger than quasar emitting regions, so this technique has limited application and dynamic range. Smaller sources such as individual stars are, of course, much fainter.

The scalar field composing these objects is so weakly coupled to the standard model that they would never be detected directly, but would only make their effect known to us gravitationally. Thus the rich substructure of the halo dark matter does not have other effects, such as gamma ray annihilation signatures or clustering in direct detection experiments, that occur for other dark matter candidates. The main exception to note is the possibility of ScaMs of classical invisible axions, which could show up in direct detection as clumping in time as well as energy.

ScaM particles when they condense are moving with modestly relativistic velocities in spatially coherent streaming flows on the scale of the nonlinear lumps at that time. These redshift by the time of the nonlinear collapse so that they do not prevent collapse, but it is worth mentioning that they do not have the dynamically-cold classical distribution function characteristic of homogeneous axion condensation. The broader coarse grained distribution function could in principle have some dynamical effects, which are too subtle to model in our simulations.

The scalar field collapses into ScaMs at matter-radiation equality, seeding early bottom up hierarchical structure formation as successively larger mass scales become virialized. This in turn results in early star formation, with baryon accretion onto the ScaMs starting as early at $z \sim 1400$ for a ScaM mass near the cosmological limit at $M_{ScaM} \sim 4 \times 10^3 M_\odot$. This could have substantial observational effects on energy input into diffuse gas, affecting the epoch of reionization, and possibly also direct detection of early stellar systems. The reionization epoch is already being probed by quasar absorption to $z > 6$ and by CMB polarization to $z > 10$; even larger redshifts may become accessible in the future to similar techniques, as well as direct 21cm mapping. These more indirect effects are of course more complicated to model than the more direct influence of the lensing.

The nature of the dark matter remains unknown to us. Scalar fields play an important role in cosmology, being front and center in viable models of inflation and many theories of the dark energy. We have shown here that, should a scalar field also contribute to solving the dark matter mystery, it is a good candidate for large isocurvature fluctuations which cause them to collapse into dense ScaMs; in fact, though the scalar may live in a hidden sector extremely weakly coupled to us, so that we would detect no direct particle interactions, gravitational

lensing may provide us a probe into this sector.

Acknowledgments

This work was supported by NSF grant AST-0098557 at the University of Washington.

APPENDIX: LATE PHASE TRANSITIONS IN AXION COSMOLOGY

We demonstrate a technically natural model which provides a phase transition well below the QCD scale, seeding density fluctuations in both Higgs-like and axion-like fields. This model was motivated in ref. [24] for the purpose of demonstrating that in theories where the axion's decay constant evolves after the QCD phase transition, the cosmological upper bound on the axion decay constant, $f_a \lesssim 10^{12}$ GeV, does not apply. The model as written here applies specifically to the QCD axion, but the model can be generalized to any set of scalar fields, not necessarily connected with the solution of the strong CP problem.

The phase transition in this model is driven by a complex field ϕ , whose radial mode has a Higgs-like potential,

$$V(\phi) = \mu^4 \left| \frac{\phi^2}{M^2} - 1 \right|^2, \quad (\text{A.1})$$

where we require $\mu^2/M \ll H(T_{QCD})$ in order that the vacuum expectation value (vev) of the field remain frozen at its initial position, away from the minimum of the potential at $\langle \phi \rangle = M$, until $T < T_{QCD}$. The field ϕ is coupled to the Peccei-Quinn (PQ) sector through a potential

$$V(\phi, X_1, X_2) = \lambda^2 |hX_1X_2 - \phi^2|^2, \quad (\text{A.2})$$

where X_1 and X_2 carry opposite PQ charges. X_1 is the standard PQ field coupled to gluon field strength through the term

$$X_1 G \tilde{G}, \quad (\text{A.3})$$

where the usual PQ potential fixes the vev $|X_1| = f_1$ when the PQ symmetry breaks at temperatures $T \gg T_{QCD}$. At the QCD phase transition, the axion gains a mass $m_a \sim m_\pi f_\pi / f_1$, and a dark matter condensation of axions forms.

A phase transition occurs when $m_\phi \sim H(T)$, so that ϕ rolls out to the minimum of its potential at $|\phi| = M$; $|X_2|$ then follows the flat direction in eqn. A.2 to a vev $f_2 = M^2/hf_1$, where the hierarchy $f_2 \gg M \gg f_1$ is assumed. It can then be shown (see [24] for details) that the energy density in the axion dark matter is transferred into the heavier pseudo-scalar $\pi_1 \equiv f_1 \text{Arg}(X_1)$, having mass $m_{\pi_1} \sim \lambda M^2/f_1$ generated at the phase transition.

As a result of the phase transition, there are two dark matter candidates in this model, one Higgs-like and one axion-like. At the phase transition, the Higgs-like mode $|\phi|$ releases energy μ^4 which subsequently redshifts like dark matter, and may be cosmologically abundant. It is so weakly coupled to ordinary matter that it may only be detected gravitationally. It has $\mathcal{O}(1)$ density perturbations resulting from the phase transition at a temperature $T \ll T_{QCD}$, which collapse into Higgs-like ScaMs with mass much larger than an axion minicluster, $M_{ScaM} \gg 10^{-12} M_\odot$. The axion-like pseudoscalar π_1 may also be cosmologically populated, and collapses into axion-like ScaMs. The mass of these ScaMs is much larger than QCD axion miniclusters as the pseudo-Goldstone boson in this model has an additional mass generated at the phase transition $m_{\pi_1}/m_a 10^{-12} M_\odot \gg 10^{-12} M_\odot$.

There is a mechanism in this model which allows for equal cosmological abundances of Higgs-like and axion-like dark matter, ϕ and π_1 , without any fine-tuning. At the QCD phase transition, π_1 dark matter is produced with energy density

$$\rho_{\pi_1}(T) = m_{\pi_1} n_{\pi_1}, \quad (\text{A.4})$$

where n_{π_1} is the number density, which dilutes as T^3 , and m_{π_1} now receives a contribution from its mixing with ϕ :

$$m_{\pi_1}^2(\phi) \sim \frac{m_\pi^2 f_\pi^2}{f_1^2} + \frac{\lambda^2 \langle |\phi| \rangle^4}{f_1^2}, \quad (\text{A.5})$$

This creates an effective potential for ϕ ,

$$V_{eff}(\phi) = m_{\pi_1}(\phi) n_{\pi_1}. \quad (\text{A.6})$$

This effective potential will delay the temperature of the phase transition, when ϕ rolls to $\langle |\phi| \rangle = M$, until π_1 has diluted enough that $V_{eff}(M) < \mu^4$. At that point the energy densities in the ϕ and π_1 fields are equal, and they redshift concomitantly so that their energy densities remain equal thereafter. This gives rise to the possibility of the cosmological presence of both Higgs-like and axion-like miniclusters. As the Higgs-like and axion-like miniclusters have different typical densities (the latter often being 10^4 times more dense, as explained in Sec. III), this implies a potentially varied cosmic population reachable by lensing experiments on different scales.

We also wish to emphasize that the physical features discussed here of late scalar field phase transitions are quite generic and independent of the presence of axions; however, the axion model provides a motivation to consider such phase transitions around the QCD time, as well as illustrates a model with all the physical features discussed in this paper.

-
- [1] G. Bertone, D. Hooper, and J. Silk, *Phys. Rept.* **405**, 279 (2005), hep-ph/0404175.
 - [2] S. Eidelman, K. Hayes, K. Olive, M. Aguilar-Benitez, C. Amsler, D. Asner, K. Babu, R. Barnett, J. Beringer, P. Burchat, et al., *Physics Letters B* **592**, 1+ (2004), URL <http://pdg.lbl.gov>.
 - [3] C. Alcock et al. (MACHO), *Astrophys. J.* **542**, 281 (2000), astro-ph/0001272.
 - [4] A. Udalski et al., *Acta Astron.* **52**, 1 (2002), astro-ph/0202320.
 - [5] E. Aubourg et al., *Nature* **365**, 623 (1993).
 - [6] P. Tisserand et al. (EROS-2) (2006), astro-ph/0607207.
 - [7] D. P. Bennett et al., *Astrophys. J.* **579**, 639 (2002), astro-ph/0109467.
 - [8] A. Rest et al., *Astrophys. J.* **634**, 1103 (2005), astro-ph/0509240.
 - [9] E. A. Baltz and L. Hui, *Astrophys. J.* **618**, 403 (2005).
 - [10] M. A. Walker and G. F. Lewis, *Astrophys. J.* **589**, 844 (2003).
 - [11] J. J. Dalcanton, C. R. Canizares, A. Granados, C. C. Steidel, and J. T. Stocke, *Astrophys. J.* **424**, 550 (1994).
 - [12] J. S. B. Wyithe and A. Loeb, *Astrophys. J.* **577**, 57 (2002).
 - [13] C. C. Wiegert, Ph.D. Thesis (2003).
 - [14] M. R. S. Hawkins, *MNRAS* **278**, 787 (1996).
 - [15] E. A. Baltz et al., *Astrophys. J.* **610**, 691 (2004), astro-ph/0310845.
 - [16] C. J. Hogan and M. J. Rees, *Phys. Lett.* **B205**, 228 (1988).
 - [17] E. W. Kolb and I. I. Tkachev, *Phys. Rev. Lett.* **71**, 3051 (1993), hep-ph/9303313.
 - [18] E. W. Kolb and I. I. Tkachev, *Phys. Rev.* **D50**, 769 (1994), astro-ph/9403011.
 - [19] E. W. Kolb and I. I. Tkachev, *Astrophys. J.* **460**, L25 (1996), astro-ph/9510043.
 - [20] M. Y. Khlopov, A. S. Sakharov, and D. D. Sokoloff, *Nucl. Phys. Proc. Suppl.* **72**, 105 (1999).
 - [21] A. S. Sakharov, D. D. Sokoloff, and M. Y. Khlopov, *Phys. Atom. Nucl.* **59**, 1005 (1996).
 - [22] A. S. Sakharov and M. Y. Khlopov, *Phys. Atom. Nucl.* **57**, 485 (1994).
 - [23] J. Yoo, J. Chaname, and A. Gould, *Astrophys. J.* **601**, 311 (2004), astro-ph/0307437.
 - [24] D. B. Kaplan and K. M. Zurek, *Phys. Rev. Lett.* **96**, 041301 (2006), hep-ph/0507236.
 - [25] J. A. Frieman, C. T. Hill, A. Stebbins, and I. Waga, *Phys. Rev. Lett.* **75**, 2077 (1995), astro-ph/9505060.
 - [26] W. H. Press, B. S. Ryden, and D. N. Spergel, *Phys. Rev. Lett.* **64**, 1084 (1990).
 - [27] J. A. Frieman, C. T. Hill, and R. Watkins, *Phys. Rev.* **D46**, 1226 (1992).
 - [28] C. J. Hogan, *Phys. Rev. Lett.* **74**, 3105 (1995), astro-ph/9412054.
 - [29] A. H. Guth and S.-Y. Pi, *Phys. Rev.* **D32**, 1899 (1985).
 - [30] P. McDonald, U. Seljak, R. Cen, D. Shih, D. H. Weinberg, S. Burles, D. P. Schneider, D. J. Schlegel, N. A. Bahcall, J. W. Briggs, et al., *Astrophys. J.* **635**, 761 (2005), astro-ph/0407377.

- [31] P. McDonald, U. Seljak, S. Burles, D. J. Schlegel, D. H. Weinberg, R. Cen, D. Shih, J. Schaye, D. P. Schneider, N. A. Bahcall, et al., *Astrophys. J. Supp.* **163**, 80 (2006), astro-ph/0405013.
- [32] P. McDonald, J. Miralda-Escudé, M. Rauch, W. L. W. Sargent, T. A. Barlow, R. Cen, and J. P. Ostriker, *Astrophys. J.* **543**, 1 (2000), astro-ph/9911196.
- [33] N. Afshordi, P. McDonald, and D. N. Spergel, *Astrophys. J.* **594**, L71 (2003), astro-ph/0302035.
- [34] J. M. Bardeen, J. R. Bond, N. Kaiser, and A. S. Szalay, *Astrophys. J.* **304**, 15 (1986).
- [35] B. Paczynski, *Astrophys. J.* **304**, 1 (1986).
- [36] J. W. Wadsley, J. Stadel, and T. Quinn, *New Astronomy* **9**, 137 (2004).
- [37] M. Bartelmann and P. Schneider, *Phys. Rept.* **340**, 291 (2001), astro-ph/9912508.
- [38] J. Diemand, B. Moore, and J. Stadel, *Nature*. **433**, 389 (2005), astro-ph/0501589.
- [39] E. Ripamonti and T. Abel (2005), astro-ph/0507130.
- [40] T. Abel, G. L. Bryan, and M. L. Norman, *Science* **295**, 93 (2002), astro-ph/0112088.
- [41] N. Yoshida, T. Abel, L. Hernquist, and N. Sugiyama, *Astrophys. J.* **592**, 645 (2003), astro-ph/0301645.
- [42] R. Barkana and A. Loeb, *Phys. Rep.* **349**, 125 (2001).
- [43] P. Arras and I. Wasserman (1998), astro-ph/9811370.
- [44] B. Moore, *Astrophys. J.* **413**, L 93 (1993), astro-ph/9306004.
- [45] J. Yoo, J. Chanamé, and A. Gould, *Astrophys. J.* **601**, 311 (2004), astro-ph/0307437.